Proceedings of the ASME 2017 International Design Engineering Technical Conferences and Computers and Information in Engineering Conference
IDETC/CIE 2017
August 6-9, 2017, Cleveland, Ohio, USA

DETC2017-67197

SELF-LOCKING ORIGAMI STRUCTURES AND LOCKING-INDUCED PIECEWISE STIFFNESS

Hongbin Fang*, Shih-Cheng A. Chu, K.W. Wang

Department of Mechanical Engineering
University of Michigan
Ann Arbor, MI 48105, USA

ABSTRACT

The folding motion of an origami structure can be stopped at a non-flat position when two of its facets bind together. Such facet-binding will induce *self-locking* so that the overall origami structure can stay at a pre-specified configuration without the help of additional locking devices or actuators. This research investigates the designs of self-locking origami structures and the locking-induced kinematical and mechanical properties. We show that incorporating multiple cells of the same type but with different geometry could significantly enrich the self-locking origami pattern design. Meanwhile, it offers remarkable programmability to the kinematical properties of the self-locking origami structures, including the number and position of locking points, and the deformation range. Self-locking will also affect the mechanical characteristics of the origami structures. Experiments and finite element simulations reveal that the structural stiffness will experience a sudden jump with the occurrence of self-locking, inducing a piecewise stiffness profile. The results of this research would provide design guidelines for developing self-locking origami structures and metamaterials with excellent kinematical and stiffness characteristics, with many potential engineering applications.

1. INTRODUCTION

Origami-based folding mechanisms have been adopted in a wide variety of engineering structures, ranging from biomedical devices [1–3], printable robots [4,5], sandwich panels [6], actuators [7], and large-scaled aerospace [8,9] and architectural elements [10]. Recently, origami also demonstrates its great values in developing mechanical metamaterials. By programming the origami crease pattern, the metamaterials' kinematical and mechanical properties can be tailored within a large design space. By employing the origami folding algorithms, extraordinary characteristics that are unseen in traditional materials can be achieved, such as auxetic effects [11–13], multistability [13–16], recoverable collapse[17], and reprogrammable stiffness [18]. Rigid-foldable origami is the main subset of folding pattern in the abovementioned examples, where the folding only involves crease hinge rotations without deforming the polygon facets.

Note that the origami cannot necessarily be folded flat (i.e., with flat-foldability), rather, certain origami structures may stay at a particular configuration and cannot be folded further. Such feature is named as "locking". There are various mechanisms that can trigger origami locking. For example, if the origami facet thickness is not negligible, the facets may come into contact and stop folding, even though the corresponding zero-thickness kinematical model does not predict facet intersection. In addition, the facet thickness may deviate the hinge location from the ideal place and limit the folding process by generating a locking state. Typically, such locking shows negative effect because the achievable folding range is reduced. Different techniques have been suggested to avoid the locking and to regain the full range of folding [19,20]. However, prescribed and controllable locking would become beneficial or even indispensable in applications like self-deployable structures [8,9] and self-folding devices [2,3], because it endows the origami structures with the crucial ability to limit folding and to stay at a desired configuration. Several designs have been proposed to achieve controllable locking by introducing additional locking devices. For example, in some micro-self-folding systems, self-aligned locking hinges made of solder are employed at the edges of origami panels to ensure pre-specified folding angles and improve the mechanical strength of the

* Address all correspondence to this author: hongbinf@umich.edu

structure [3,21]. In another case, a combination of shape memory alloys (SMAs) and shape memory polymers (SMP) were adopted to create a self-folding laminate with controllable locking ability, where the SMA functions as an actuator to generate folding, while the SMP locks the achieved deformation [22].

Other than relying on additional devices or active materials, controllable locking can also be achieved by harnessing the intrinsic *facet-binding* effect during origami folding. In a generic degree-4 vertex (for short, 4-vertex) origami, there exists a crease that is capable of fully closing while others are not, so that the two facets astride this crease will bind together and stop further folding. Such locking mechanism does not require additional locking devices and as a result is named as "***self-locking***" [12]. Schenk [11] and Fang et al [12,23] have demonstrated several examples of 4-vertex self-locking structures, such as origami sheet connected by two different Miura-ori units, single-collinear sheet, single-collinear stacked block, etc. Because of the underlying design simplicity and reliability, such self-locking shows great potential in developing structures and mechanical metamaterials with controllable folding deformations. However, other than the reported examples of self-locking, a comprehensive understanding of the self-locking origami is still lacking. Especially, there is a need to enrich the designs of self-locking origami and to uncover the locking-induced mechanical properties changes.

This paper will address two issues to advance the state-of-the-art knowledge: self-locking origami designs and locking-induced mechanical property changes. We will discuss two promising findings in detail. The first finding is that by incorporating multiple cells/units of the same type but with different geometry into construction, both the structure designs and the corresponding kinematical properties are significantly enriched and expanded. We show that owing to the multi-component designs, the self-locking origami structures possess great programmability in terms of the number and position of locking points and the deformation range. The second finding is the locking-induced piecewise stiffness. That is, the structure's force-displacement relation is significantly altered before and after self-locking, giving rise to a piecewise stiffness profile. The programmable self-locking origami and the piecewise stiffness can open up new possibilities for quasi-static and dynamic applications. For example, shape morphing typically requires a structure or material to change its shape between two targeted configurations with minimal actuation input, and then stay at the targeted shape while withstand high external loads [24]. Such requirements can be achieved by tailoring the crease designs so that self-locking and the corresponding stiffness jump occur at the targeted load-bearing configurations.

The rest of this paper will explore the self-locking origami designs (Section 2), analyze the kinematical performance (Section 3) and the stiffness characteristics (Section 4) originating from self-locking. Summary and discussions will be presented in Section 5.

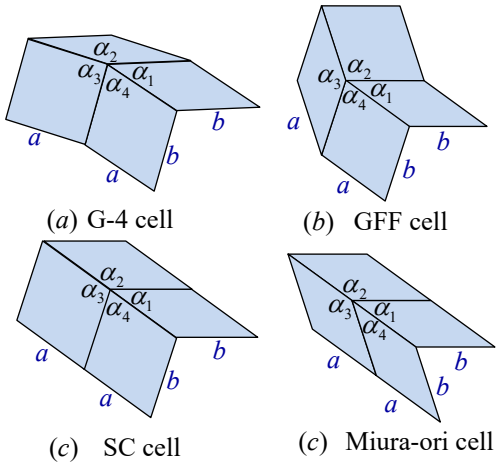

FIGURE 1. Four types of 4-vertex origami pattern. The sector angles α_i $(i=1,...,4)$ need to satisfy the geometry constraints listed in Table 1. a and b are the lengths of the parallelogram panel.

2. SELF-LOCKING ORIGAMI DESIGNS

In this section, we examine the 4-vertex origami patterns and identify those with self-locking abilities. 4-vertex origami is the simplest pattern that can be periodically tessellated in three directions and possesses only one continuous degree-of-freedom for folding [25]. It has been recognized that only a small number of 4-vertex origami patterns possess flat-foldability [12]. Figure 1 displays the geometry of different types of 4-vertex origami pattern, with their non-trivial and defining conditions being summarized in Table 1. Among these patterns, the general flat-foldable (GFF) and Miura-ori patterns are flat-foldable, while the generic 4-vertex (G-4) and single-collinear (SC) patterns would self-lock during folding.

Schenk et al. [11] and Fang et al. [12] have discovered that the same types of 4-vertex cells (except the G-4 cell owing to its inherent bending deformation) can be stacked together under geometry constraints. Particularly, although the GFF cell can be folded flat, the stacked GFF unit loses its flat-foldability due to inter-cell facet-binding [12,23]. Hence, both the SC stacked unit and the GFF stacked unit would self-lock during folding.

TABLE 1. Geometry constraints for 4-vertex origami patterns

Type	Non-trivial conditions	Defining conditions	# independent sector angles
G-4	$\sum_i \alpha_i = 2\pi$, $\alpha_j < \sum_i \alpha_{i\neq j}$	/	3
GFF		$\alpha_1+\alpha_3=\alpha_2+\alpha_4$	2
SC		$\alpha_1+\alpha_2=\alpha_3+\alpha_4$	2
Miura-ori		$\alpha_1+\alpha_3=\alpha_2+\alpha_4$, $\alpha_1+\alpha_2=\alpha_3+\alpha_4$	1

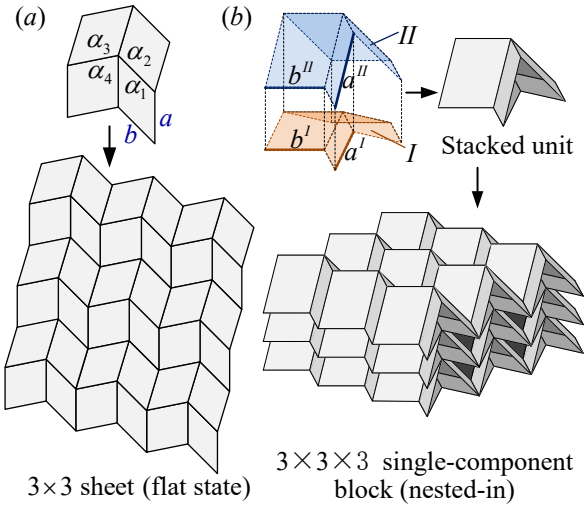

FIGURE 2. Single-component design ideas: (a) a 3×3 SC self-locking sheet, and (b) a 3×3 SC self-locking stacked block (nested-in). Construction of stacked unit is illustrated in (b), see details in [26].

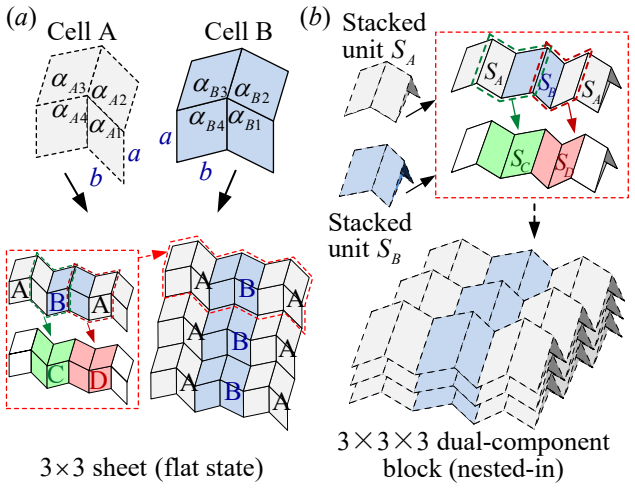

FIGURE 3. Dual-component design idea. As an example, (a) displays a dual-component SC self-locking sheet, and (b) shows a dual-component SC self-locking stacked block (nested-in). Note that at the connections new types of cell and stacked units are generated, see details in [26].

Therefore, in this study, G-4 and SC cells, as well as the GFF and SC stacked units are employed for constructing self-locking structures. By repeating the G-4 and SC cells in two directions in a plane, 2-dimensional (2D) self-locking sheets can be generated. By repeating the GFF and SC stacked unit in three directions, 3-dimensional (3D) self-locking blocks can be set up. If only one kind of cell (or stacked unit) is employed in the construction, the self-locking characteristics will be correspondingly transmitted from the cells (or stacked units) to the sheets (or blocks). Such single-component design ideas are illustrated in Figure 2, with a SC sheet and SC stacked block as examples.

On the other hand, cells or stacked units of the same type but with different geometry can be incorporated for construction if extra geometry constraints are satisfied [26]. Figure 3 shows the dual-component design idea, with a dual-component SC sheet (composed of SC cells A, B) and a dual-component SC stacked block (composed of SC stacked units S_A and S_B) as examples. Note that new cells (say, cells C and D) or new staked units (say, units S_C and S_D) will be generated at the connections, which, interestingly, are of the different types as the component cells or units. For example, connecting two different G-4 cells together, the middle cells (C and D) can be either G-4 or GFF; connecting two different SC cells together, the middle cells can be either SC or Miura-ori. However, connecting two different GFF cells together, the middle cells can only be G-4; and connecting two different Miura-ori cells together, the middle cells can only be SC. In sum, there are a total of 10 different cases of dual-component sheets, see Table 2, which is significantly more abundant than single-component designs. Particularly, we note that connecting two flat-foldable cells (i.e., GFF or Miura-ori cells) will generate G-4 or SC cells at the connections, which offers additional self-locking ability. Similarly, as summarized in Table 3, new stacked units S_C and S_D can be of different types as S_A and S_B, giving the Miura-ori stacked blocks additional self-locking ability.

TABLE 2. Self-locking abilities in 4-vertex single-component and dual-component sheets

Component cell type	Single-component design	Dual-component design		
		Cell C	Cell D	Self-locking
G-4	√	GFF	GFF	√
		GFF	G-4	
		G-4	GFF	
		GFF	GFF	
GFF	×	G-4	G-4	√
SC	√	SC	SC	√
		Miura	SC	
		SC	Miura	
		Miura	Miura	
Miura-ori	×	SC	SC	√

Tables 2 and 3 reveal the advantages of incorporating two components into the construction of sheets and stacked blocks: (*i*) the design richness is significantly improved; (*ii*) the dual-component sheets or blocks acquire additional self-locking abilities because self-locking cells or self-locking stacked units are generated at the interface, although the component cells or stacked units are flat-foldable.

Remark 1: To understand the folding and self-locking behaviors of the sheets and stacked blocks, it is necessary to identify the crease that first binds (i.e., the global binding fold).

TABLE 3. Self-locking abilities in 4-vertex single-component and dual-component stacked blocks

Component stacked unit type	Single-component design	Dual-component design		
		Stacked units C and D Type		Self-locking
G-4	geometry incompatible			
GFF	√	geometry incompatible		
SC	√	SC	SC	√
		Miura	SC	
		SC	Miura	
		Miura	Miura	
Miura-ori	×	SC	SC	√

Through spherical trigonometry, the dihedral angle at each crease can be obtained, and the global binding fold can be determined [26].

Remark 2: Theoretically, self-locking structures can be constructed with more than two component cells (or stacked units). However, incorporating more components will not alter or enrich the locking behavior, or generate new types of cell (or stacked unit); rather, it will complicate the structure design and manufacturing. Hence, only single- and dual- component structures are considered in this research.

3. PROGRAMMABLE KINEMATICAL PROPERTIES

In this section, we discuss how the dual-component designs contribute to the kinematical properties of the self-locking origami structures. The following indexes are employed for evaluation.

- ***Locking point.*** Locking points indicate the locations where facet-binding happens, i.e. the locations where the global binding folds locate.
- ***Flat-folded locking plane.*** In a dual-component structure, if the global binding folds locate in flat-foldable cells or flat-foldable stacked units (even though the sheet or the block as a whole does not possess flat-foldability), flat-folded locking planes can be generated, which is a particular type of locking point.
- ***Deformation range.*** The deformation range is defined as $\eta = (L_0 - L_f)/L_0$, where L_f is the length of the structure when self-locking occurs, and L_0 is the initial length when the origami sheet (or the bottom cells of the stacked unit) is flat.

The above three indexes have important implication in engineering applications. The number of locking points and their locations are necessary information for the utilization of self-locking structures. For example, active materials or actuators are normally set at the locking points for effective actuation and folding; the material at the locking points needs careful selection to prevent damage or failure and to tailor the structure's mechanical property. The number of flat-folded planes would significantly influence the structure's folding ability. The deformation range η measures the deformability

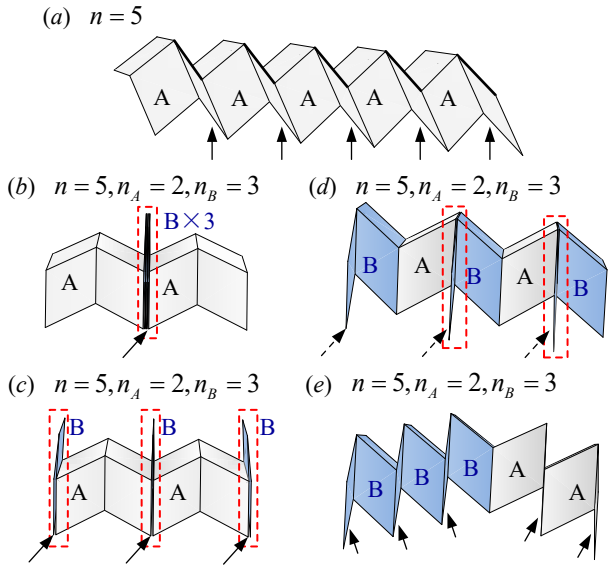

FIGURE 4. Illustration of programmable locking points and flat-folded locking planes in self-locking sheets. The locking points are indicated by arrows, and the flat-regions are indicated by dashed rectangles. (a) Single-component sheet. (b) and (c) Dual-component sheet composed of two different Miura-ori cells, with one and three locking points (flat-folded locking plane), respectively. (d) and (e) Dual-component sheet composes of two different SC cells. In (d) the sheet has three locking points (flat-folded planes), and in (d) the sheet has five locking points, but none of them is flat-folded locking plane.

of the self-locking structure; the larger the value is, the stronger its deformability.

For single-component designs, the number and position of locking points are fixed, and flat-folded locking planes cannot be generated. The deformation range of a single-component self-locking keeps the same as the component unit and lacks programmability. As an example, Figure 4(a) shows a 5×1 single-component sheet at its self-locking configuration, where locking points are observed in each component unit.

Due to the introduction of an additional component, the kinematical properties can be programmed extensively by employing different tessellations, without changing the components. For example, we use 2 Miura-ori cells A and 3 Miura-ori cells B to construct a 5×1 dual-component sheet. SC cells are generated at the connections between cells A and B. With different tessellations, one locking point (Figure 4(b)) and three locking points (Figure 4(c)) are achieved in the sheet, and their locations are at different places. Particularly, since the global binding fold locates in Miura-ori cell B, it works as the flat-folded locking plane in the sheets. In another example, we connect 2 SC cells A and 3 SC cells B to construct a 5×1 dual-component sheet. In this case, the newly generated cell at the connection between cells A and B becomes flat-foldable Miura-

Design	Type	Locking points #	Flat-folded locking plane	Deformation range
Single-component sheet	G-4	n	×	η_A
	GFF	flat-foldable		1
	SC	n	×	η_A
	Miura-ori	flat-foldable		1
Dual-component sheet	G-4	$[n_A \text{ or } n_B,\ n]$	possible	$(\eta_A,\ \eta_B)$
	GFF	$[1,\ \min\{n_A, n_B\}(+1)]$	possible	$(\eta_A \text{ or } \eta_B,\ 1)$
	SC	$[n_A \text{ or } n_B,\ n]$	possible	$(\eta_A,\ \eta_B)$
	Miura-ori	$[1,\ \min\{n_A, n_B\}(+1)]$	possible	$(\eta_A \text{ or } \eta_B,\ 1)$
Single-component stacked block	G-4	geometry incompatible		
	GFF	n	×	η_A
	SC	n	×	η_A
	Miura-ori	flat-foldable		1
Dual-component stacked block	G-4	geometry incompatible		
	GFF	geometry incompatible		
	SC	$[n_A \text{ or } n_B,\ n]$	possible	$(\eta_A,\ \eta_B)$
	Miura-ori	$[1,\ \min\{n_A, n_B\}(+1)]$	possible	$(\eta_A \text{ or } \eta_B,\ 1)$

TABLE 4. Kinematical properties of self-locking sheets and stacked blocks. In the table, n_A and n_B denote the number of cells (or stacked units) A and B (S_A and S_B), $n = n_A + n_B$ is the total number of cells (stacked units). η_A and η_B denote the deformation range of component cells (stacked units) A and B (S_A and S_B) [26]

ori. By tessellating the cells, we could obtain three locking points (three flat-folded planes) (Figure 4(d)) or five locking points (Figure 4(e)) in the sheet.

Table 4 summarizes the kinematical characteristics of the single-component and dual-component structures [26].

4. LOCKING-INDUCED PIECEWISE STIFFNESS

In addition to the kinematical characteristics, the change on mechanical properties is also of our interest. Here we discuss how the structural stiffness changes due to self-locking.

4.1 Origami Structure with Negligible Facet-Thickness and Pre-Locking Rigid-Foldability

We first consider the case that the origami facet thickness is thin and can be neglected, and the facet material is much stiffer than the crease material. Hence before self-locking happens, i.e., during the pre-locking stage, the origami structure deforms following exactly the kinematical algorithm of rigid folding: that is, the crease material bends like flexible hinges but the facet material remain undeformed. The overall structure tangent stiffness comes from the bending stiffness of the crease lines [15,25,27]. After self-locking, the structure cannot be rigidly folded any more, and further loading will instead directly deform the facet materials, which gives rise to much higher stiffness. As the kinematic relationship of rigid-folding is no longer valid, estimating the increased stiffness after self-locking would require finite-element analyses (FEA) [28] or via experiments [29]. In this research, we design and fabricate a prototype for our experimental investigation.

A SC stacked unit prototype is fabricated. The origami facets are water jet cut out of steel plates (with thickness 0.254mm), and the creases are made of adhesive-back polyethylene films (with thickness 0.127mm). With such a setup, the facets (steel) are much stiffer than the creases (polyethylene) so that the prototype retains rigid-foldability during the pre-locking stage; the facets and creases are thin enough so that the kinematical folding algorithm can be ensured. Meanwhile, pre-folded spring-steel stripes (with thickness 0.18 mm) are applied to certain crease lines to generate some bending stiffness (see schematic illustration in the inset of Figure 5(a)). We perform eight compression tests on the prototype in its length direction. Figure 5(a) shows the measured force–displacement curve and the standard deviations (shades). The curve consists of two segments with significantly different slopes. Linear regression is performed on the two curve segments to obtain the corresponding approximated structure stiffness (Figure 5(b)). Agreeing with the prediction, we find that the overall stiffness experiences a significant jump from 0.877 N/mm to 104.6 N/mm (>100 times) due to self-locking. Figure 5(c) displays the photos of the SC stacked unit prototype before (*i*), at (*ii*), and after self-locking (*iii*). It is observed that at the pre-locking stage, the steel facets keep undeformed, while at the post-locking stage the steel facets show obvious bending, which accounts for the sharp stiffness jump.

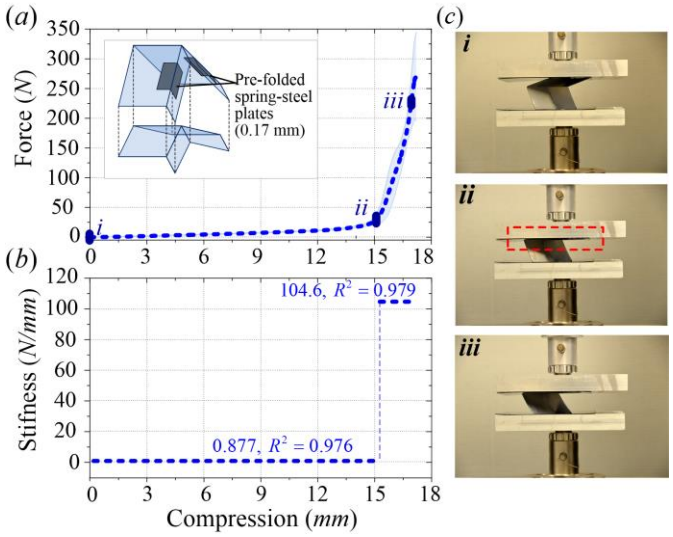

FIGURE 5. Compression tests on a SC stacked unit prototype (nested-in configuration). (a) Force–displacement curve, with inset showing the positions where spring-steel plates are pasted. (b) Stiffness obtained through linear regression, the stiffness values and the coefficient of determination (R^2) are given. (c) Photos of the prototype at three configurations ***i***, ***ii*** and ***iii***; the binding facets at the self-locking instant (***ii***) are denoted by dashed rectangle.

4.2 Origami Structure with Flexible and Thick Facets

If origami folding algorithms are applied to engineering structures such as roofs, solar panels, and space mirrors, the facet and crease thickness normally cannot be disregarded. If origami patterns are employed to develop mechanical metamaterials through advanced manufacture techniques, using single-component flexible material is beneficial and attractive. Therefore, this subsection discusses another case where the origami facets are made of soft, flexible materials and their thickness cannot be neglected. In such a case, the facets may be deformed (bended, twisted, or stretched) during folding because they are not significantly stiffer than the creases, and as a result the origami's folding will not exactly follow the rigid folding kinematic algorithm. Hence, both the facets and crease materials would contribute to the structural compliance/ stiffness, no matter before or after self-locking. To explore the structural stiffness of such origami structures, experiments and finite element analysis (FEA) are carried out.

3D-printed prototype and test. We first build a 3D origami model, shown in Figure 6(a), whose zero-thickness counterpart is a SC stacked unit. The crease thickness (2 *mm*) is set to be much thinner than the facet thickness (5 *mm*). The facets and creases are carefully shaped, rounded, and offset to allow folding, and the materials at the vertices are removed to prevent generating large strains. Meanwhile, two supports are designed for installation purpose; they are connected with the SC prototype with very thin creases (1 *mm*) so that its in-plane shear deformation [12] will not be completely prohibited (see

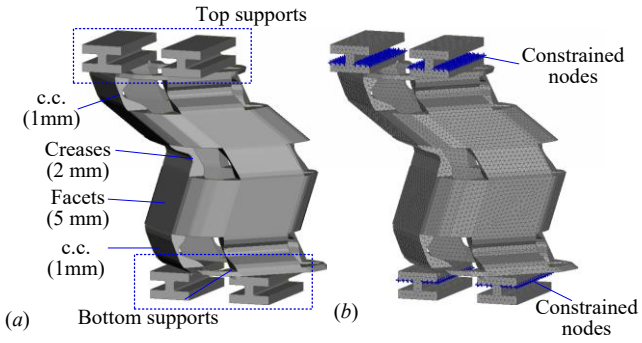

FIGURE 6. 3D model of a SC stacked unit (a) and the corresponding FE model (b). In (a), "c.c." indicates the connecting creases between the supports and the SC stacked unit. In (b), the constrained nodes are denoted.

the connecting creases 'c.c.' in Figure 6(a)). Based on this model, a prototype is 3D-printed with flexible photopolymer resin.

We perform five compression tests on the prototype. Figure 7(a) shows the measured force-displacement curve (solid). It reveals that the experimental force-displacement curve consists of two segments with obviously different slopes. Similarly, linear regression of the two curve segments gives the corresponding structure stiffness (Figure 7(b), solid), which shows an obvious jump due to self-locking (from 0.5 N/mm to 1.35 N/mm). Figure 7(c) displays the photos of the 3D-printed prototype before (*i*), at (*ii*), and after self-locking (*iii*). It is observed that unlike the steel prototype reported in subsection 4.1, the origami facets begin to deform during the pre-locking stage; when certain facets bind with others, obvious deformation of the facets and crease occur. Note that in this case the self-locked stiffness value is much lower than that of the steel prototype because the 3D printing material is much softer than steel.

Finite Element Analysis (FEA). The finite element method is used with Abaqus to simulate the stiffness change caused by self-locking. The 3D model (Figure 6(a)) is discretized using tetra-4 elements of side length 0.75mm (Figure 6(b)). Hyper-elastic material is assumed for the simulation using the Neo-Hookean model. Constraints are set on the support panels to ensure that they can only move in the vertical direction by bounding the nodes completely in all other degrees of freedom (Figure 6(b)). To include the locking-induced effects into the numerical simulations, general contact is defined for the whole model, in which the contact domain includes all element-based surfaces. Analyses under implicit quasi-static uniaxial compression are performed with displacement control acting on the panels of the support.

The Finite Element Analysis (FEA) provides us with the simulated force-displacement curve (Figure 7(a), dashed), and through linear regression we obtain the approximated stiffness (Figure 7(b), dashed). We find that FEA simulation also shows a piecewise stiffness profile, with a locking-induced jump

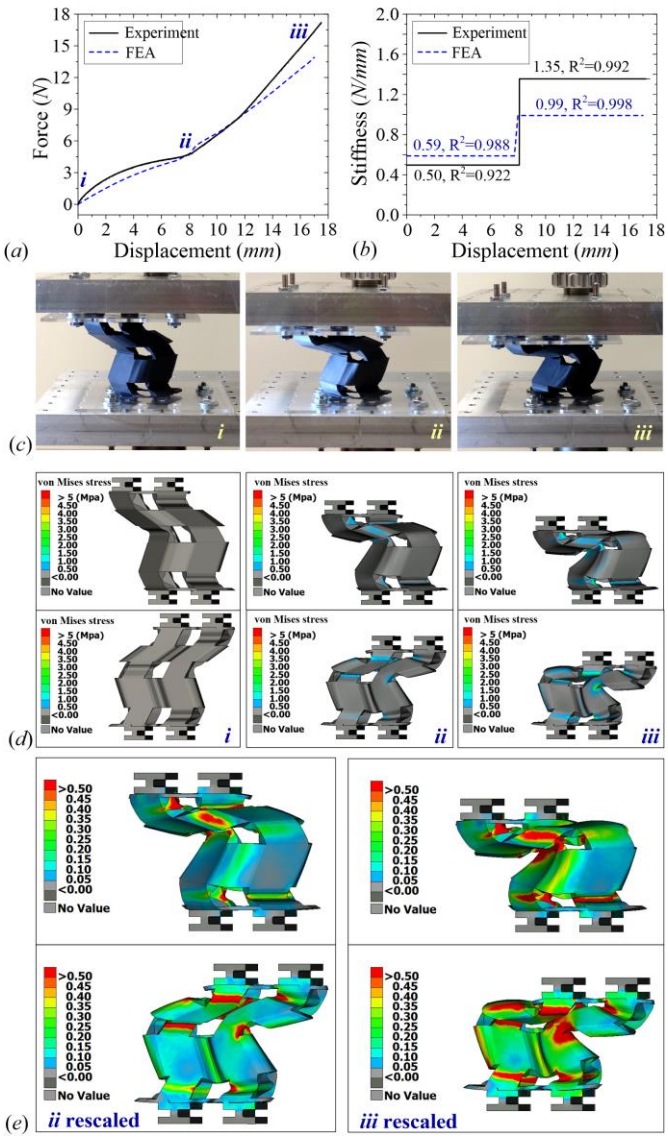

FIGURE 7. Experiment and FEA results. (a) Experimental (solid) and simulated (dashed) force-displacement curves, where ***i***, ***ii***, and ***iii*** indicate the initial configuration, the self-locked instant, and the post-locked configuration, respectively. (b) Experimental (solid) and simulated (dashed) stiffness obtained through linear regression; the coefficients of determination (R^2) are given. (c) Photos of the 3D-printed prototype at the ***i***,***ii***,and ***iii*** configurations. (d) von Mises stress distribution in the FE model at the ***i***,***ii***, and ***iii*** configurations; the front (top) and back (bottom) views are shown. (e) *ii* and *iii* configurations with rescaled color bands.

(from 0.59 N/mm to 0.99 N/mm). The FEA predictions agree well with the experimental results in terms of the transition point, the force values, and the stiffness values. Moreover, Figure 7(d) display the von Mises stress distributions before (*i*), at (*ii*), and after (*iii*) self-locking. Particularly, we rescale the color to clearly show the stress in the facets (Figure 7(e)). It shows that at the instant of self-locking, the facets are already deformed and generate non-zero stress, which agrees with the experimental observation and indicates the difference with the steel prototype. After self-locking happens, both the creases and facets keep deforming, and the creases experience much larger deformation and generate much higher stresses than the facets. The stress concentration at the creases indicates the necessity for further optimization of the design and careful selection of the crease material in future studies.

The above experimental and FEA studies demonstrate that self-locking and locking-induced stiffness jump also exist in origami prototype with flexible and thick facets. Meanwhile, it is found that the prototype behaved consistently during the five tests and was not damaged under large deformation. These observations pave the way for rapid manufacturing self-locking origami metamaterials with soft materials though 3D-printing techniques.

5. SUMMARY AND DISCUSSION

This research investigates a new category of origami structures with self-locking abilities. Here, the self-locking can be achieved without any additional locking devices or actuators but by making use of the facet-binding effect. In addition to and advancing from a single-component design, we incorporate two component cells of the same type but with different geometry into the construction. We show that such dual-component design could produce a wider variety of sheets and stacked blocks than using single-component design. In addition, we gain new knowledge that through different cell tessellations, the dual-component design offers excellent programmability on the structures' kinematical properties, including the number and position of flat-folded locking planes and locking points, and the deformation range. Such programmability cannot be achieved in single-component structures.

Self-locking will also alter the origami structures' stiffness properties. To demonstrate this point, a prototype with negligible facet-thickness and pre-locking rigid-foldability and a prototype with flexible and thick facets are fabricated and tested. Experiments and FEA reveal that before self-locking happens, folding is the main deformation of the structure, giving rise to relatively low structure stiffness; after self-locking happens, folding will be largely limited, but the facet or crease bending/twisting will happen and significantly increase structure stiffness. Particularly, the 3D-printed prototype demonstrates the feasibility of using 3D-printing techniques and flexible materials to develop self-locking origami metamaterials with piecewise stiffness profile.

The exhibited locking-induced stiffness jump and self-locking stiffness can be further enriched if we incorporate more than two cells (or stacked units) with different stiffness profiles into the design. Theoretically, a self-locking origami structure composed of n cells (or n stacked units) with n different stiffness profiles is able to exhibit 2^n stiffness profiles by

actively locking its component cells (or stacked units) through embedded actuators.

The newly discovered programmable kinematical and stiffness properties will open up new possibilities for scientific and engineering applications of various scales. For example, aerospace foldable structures [24] typically require large deformation with minimal actuation, as well as the ability to stay at a targeted configuration and withstand external load; such requirements can be achieved by employing the self-locking structures. Locking-induced stiffness jump can also be used as an embedded safety mechanism to prevent excessive deformations, which has many applications in robotics. Furthermore, locking induced piecewise stiffness can find its value in dynamic applications such as vibration isolation [30].

ACKNOWLEDGMENTS

This research was partially supported by the National Science Foundation under Awards 1634545, the University of Michigan Mechanical Engineering Collegiate Professorship, and the University of Michigan Summer Undergraduate Research in Engineering (SURE) funding.

REFERENCES

[1] Kuribayashi, K., Tsuchiya, K., You, Z., Tomus, D., Umemoto, M., Ito, T., and Sasaki, M., 2006, "Self-deployable origami stent grafts as a biomedical application of Ni-rich TiNi shape memory alloy foil," Mater. Sci. Eng. A, **419**(1–2), pp. 131–137.

[2] Peraza-Hernandez, E. A., Hartl, D. J., Malak Jr, R. J., and Lagoudas, D. C., 2014, "Origami-inspired active structures: a synthesis and review," Smart Mater. Struct., **23**(9), p. 94001.

[3] Randall, C. L., Gultepe, E., and Gracias, D. H., 2012, "Self-folding devices and materials for biomedical applications," Trends Biotechnol., **30**(3), pp. 138–146.

[4] Felton, S., Tolley, M., Demaine, E., Rus, D., and Wood, R., 2014, "A method for building self-folding machines," Science (80-.)., **345**(6197), pp. 644–646.

[5] Zhakypov, Z., Falahi, M., Shah, M., and Paik, J., 2015, "The design and control of the multi-modal locomotion origami robot, Tribot," Proceedings of the IEEE International Conference on Intelligent Robots and Systems, Hamburg, Germany, pp. 4349–4355.

[6] Gattas, J. M., and You, Z., 2015, "Geometric assembly of rigid-foldable morphing sandwich structures," Eng. Struct., **94**, pp. 149–159.

[7] Martinez, R. V, Fish, C. R., Chen, X., and Whitesides, G. M., 2012, "Elastomeric origami: Programmable paper-elastomer composites as pneumatic actuators," Adv. Funct. Mater., **22**(7), pp. 1376–1384.

[8] Schenk, M., Viquerat, A. D., Seffen, K. a., and Guest, S. D., 2014, "Review of Inflatable Booms for Deployable Space Structures: Packing and Rigidization," J. Spacecr. Rockets, **51**(3), pp. 762–778.

[9] Lebée, A., 2015, "From folds to structures, a review," Int. J. Sp. Struct., **30**(2), pp. 55–74.

[10] Reis, P. M., López Jiménez, F., and Marthelot, J., 2015, "Transforming architectures inspired by origami," Proc. Natl. Acad. Sci., **112**(40), p. 201516974.

[11] Schenk, M., and Guest, S. D., 2013, "Geometry of Miura-folded metamaterials," Proc. Natl. Acad. Sci., **110**(9), pp. 3276–3281.

[12] Fang, H., Li, S., Ji, H., and Wang, K. W., 2016, "Uncovering the deformation mechanisms of origami metamaterials by introducing generic degree-4 vertices," Phys. Rev. E, **94**(4), p. 43002.

[13] Yasuda, H., and Yang, J., 2015, "Reentrant Origami-Based Metamaterials with Negative Poisson's Ratio and Bistability," Phys. Rev. Lett., **114**(18), p. 185502.

[14] Silverberg, J. L., Na, J., Evans, A. A., Liu, B., Hull, T. C., Santangelo, C. D., Lang, R. J., Hayward, R. C., and Cohen, I., 2015, "Origami structures with a critical transition to bistability arising from hidden degrees of freedom," Nat. Mater., **14**(4), pp. 389–393.

[15] Waitukaitis, S., Menaut, R., Chen, B. G., and van Hecke, M., 2015, "Origami Multistability: From Single Vertices to Metasheets," Phys. Rev. Lett., **114**(5), p. 55503.

[16] Li, S., and Wang, K. W., 2015, "Fluidic origami with embedded pressure dependent multi-stability: a plant inspired innovation," J. R. Soc. Interface, **12**(111), p. 20150639.

[17] Li, S., Fang, H., and Wang, K. W., 2016, "Recoverable and programmable collapse from folding pressurized origami cellular solids," Phys. Rev. Lett., **117**(11), p. 114301.

[18] Silverberg, J. L., Evans, A. A., McLeod, L., Hayward, R. C., Hull, T., Santangelo, C. D., and Cohen, I., 2014, "Using origami design principles to fold reprogrammable mechanical metamaterials," Science (80-.)., **345**(6197), pp. 647–650.

[19] Tachi, T., 2011, "Rigid foldable thick origami," Origami 5, CRC Press, pp. 253–264.

[20] Chen, Y., Peng, R., and You, Z., 2015, "Origami of thick panels," Science (80-.)., **349**(6246), pp. 396–400.

[21] Leong, T. G., Lester, P. A., Koh, T. L., Call, E. K., and Gracias, D. H., 2007, "Surface Tension-Driven Self-Folding Polyhedra," Langmuir, **23**(17), pp. 8747–8751.

[22] Felton, S. M., Tolley, M. T., Shin, B., Onal, C. D., Demaine, E. D., Rus, D., and Wood, R. J., 2013, "Self-folding with shape memory composites," Soft Matter, **9**(32), pp. 7688–7694.

[23] Fang, H., Li, S., Xu, J., and Wang, K. W., 2016, "Locking mechanisms in degree-4 vertex origami structures," Proc. SPIE 9799 Active and Passive Smart Structures and Integrated Systems, G. Park, ed., SPIE, Las Vegas, NV, p. 979910.

[24] Kuder, I. K., Arrieta, A. F., Raither, W. E., and Ermanni, P., 2013, "Variable stiffness material and structural concepts for morphing applications," Prog. Aerosp. Sci., **63**, pp. 33–55.
[25] Waitukaitis, S., and van Hecke, M., 2016, "Origami building blocks: generic and special 4-vertices," Phys. Rev. E, **93**(2), p. 23003.
[26] Fang, H., Li, S., and Wang, K. W., 2016, "Self-locking degree-4 vertex origami structures," Proc. R. Soc. A Math. Phys. Eng. Sci., **472**(2195), p. 20160682.
[27] Li, S., and Wang, K. W., 2015, "Fluidic origami: a plant-inspired adaptive structure with shape morphing and stiffness tuning," Smart Mater. Struct., **24**(10), p. 105031.
[28] Ma, J., and You, Z., 2013, "Energy Absorption of Thin-Walled Square Tubes With a Prefolded Origami Pattern—Part I: Geometry and Numerical Simulation," J. Appl. Mech., **81**(1), p. 11003.
[29] Song, J., Chen, Y., and Lu, G., 2012, "Axial crushing of thin-walled structures with origami patterns," Thin-Walled Struct., **54**, pp. 65–71.
[30] Araki, Y., Asai, T., and Masui, T., 2009, "Vertical vibration isolator having piecewise-constant restoring force," Earthq. Eng. Struct. Dyn., **39**, pp. 1505–1523.